Precise ^{210}Pb determination with high-efficiency gamma spectrometry for dating of marine sedimentary cores

M.C. Pedrosa-García [a], M. Fontela [b], B. Quintana [a,*], F. Pérez [b], G. Francés [c], T. Marcos [a]

[a] *Departamento de Física Fundamental, Laboratorio de Radiaciones Ionizantes- Datación, Universidad de Salamanca, 37008, Salamanca, Spain*
[b] *Instituto de Investigaciones Marinas, IIM-CSIC, 36208, Vigo, Spain*
[c] *Departamento de Geociencias Marinas y O.T, Universidad de Vigo, 36310, Vigo, Spain*

ARTICLE INFO

ABSTRACT

In order to establish the chronology of deep-sea sediments from high-resolution ^{210}Pb-dating, the determination of ^{210}Pb and ^{226}Ra activity concentrations needs to be improved. Gamma spectrometry allows determining simultaneously both radionuclides. However, spectrum background is still an issue to obtain high sensitivity. Four deep-sea sediment cores were dated using Mazinger, a gamma spectrometer with high-efficiency and very low-background, and the Constant Rate and Supply model was applied to obtain recent ages.

1. Introduction

Dating of coastal sedimentary cores of paleoclimatic interest for ages between 100 and 200 years is usually obtained by applying the dating models based on ^{210}Pb in excess (Mabit et al., 2014), due to its suitable half-life, $T_{1/2} = 22.23$ (12) a *(*Bé et al., 2011). For this purpose, conventional gamma spectrometry can be used (Hassan et al., 1997; Manolopoulou et al., 2003; Chen and Huh, 1999), since it allows measuring the radionuclides of the natural disintegration chains simultaneously, in particular, ^{210}Pb, ^{226}Ra, ^{214}Pb and $^{235/238}$U (Quintana et al., 2018). The resulting chronologies are validated with artificial radionuclides like ^{241}Am and ^{137}Cs (Alvarez-Iglesias et al., 2007; Leorri et al., 2014; Irabien et al., 2015; Alvarez-Vázquez et al., 2016; Sánchez-Cabeza and Ruiz-Fernández, 2012). However, when the sediment core belongs to the deep-water basins (Fontela et al., 2019), where the sedimentation rates are very low, and the influence of human activity is much lower, dating techniques with greater accuracy than conventional gamma spectrometry are required.

In this work, the dating of four sediment cores, sampled in June–July 2016 in the North Atlantic, by using high-efficiency gamma spectrometry with the Mazinger array is discussed. Mazinger (see Fig. 1) is a low-level background and high-efficiency gamma spectrometer composed of two broad-energy-range high purity germanium detectors (HPGe) with quasi-point contact and opposite windows. An active shield surrounds the HPGe detectors, which is made by two rings of anti-Compton scintillator crystals of NaI(Tl) that are read by four coupled photomultipliers

equidistantly placed at the top of each ring (Quintana et al., 2017; Britton et al., 2015). Mazinger also contains a passive shield composed, from the inner part to the outer one, by a 3-mm thick layer of electrolytic Cu, a 5-cm thick layer of ancient Pb and a 10-cm thick layer of ^{60}Co impurity-free Fe. Besides, to reduce the background produced by radon and its progenies, the inner chamber is ventilated with a constant flux of N_2 gas of 2 L/min. The equipment is located 12 m deep with respect to the ground, which reduces the cosmogenic background. All these characteristics provide us with the high efficiency, sensitivity and precision required for the dating of deep-sea sediment cores.

The ^{210}Pb dating method requires measuring a complete sequence of a sedimentary core for the determination of ^{210}Pb and ^{226}Ra activity values. The physical-mathematical models that can be applied to perform dating with ^{210}Pb are based on obtaining in-excess ^{210}Pb (^{210}Pb$_{xs}$ or ^{210}Pb$_{unsupported}$) at consecutive levels in which the core was sliced (Krishnaswamy et al., 1971; Appleby, 1998; Appleby and Oldfield, 1983). The Constant Rate of Supply (CRS) model has been widely used for sediment cores dating (Sánchez-Cabeza and Ruiz-Fernández, 2012; Sánchez-Cabeza et al., 2000). This model is based on the hypothesis that there is a constant rate of supply of unsupported or in-excess ^{210}Pb to the sediment. In-excess ^{210}Pb (^{210}Pb$_{xs}$) has to be determined taking into account that the total ^{210}Pb activity in the sediment has mainly two contributions: a direct one coming from atmospheric fall-out (^{210}Pb$_{xs}$) and an indirect one coming from the decay of the existing ^{226}Ra in the sediment, which gives rise to the supported ^{210}Pb (^{210}Pb$_{sup}$). To determine the ^{210}Pb$_{sup}$ fraction, which is given by
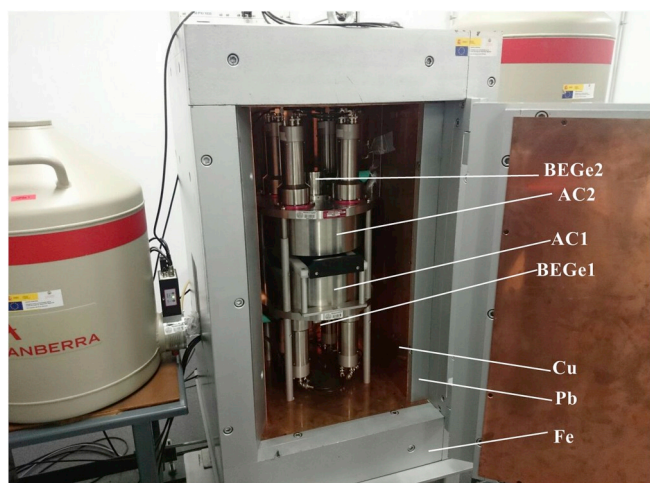

Fig. 1. Picture of Mazinger showing passive and active shielding, HPGe detectors and corresponding anti-Compton.

the ^{226}Ra activity, secular equilibrium is assumed between ^{226}Ra and ^{210}Pb$_{sup}$. This assumption has been validated by comparing their corresponding specific activities in samples where ^{210}Pb$_{xs}$ has become non-detectable.

2. Materials and methods

A total of 119 samples were analysed corresponding to four sediment box-cores recovered from three representative deep-ocean basins of the North Atlantic. Cores BC-77 (59.491; −37.6859; 3118.5 mwd) (Fontela et al., 2019) and BC-73 (59.2330; −35.1142; 3000.0 mwd) were retrieved from the Irminger Basin, located between the continental margin of Greenland and the Reykjanes Ridge. Cores BC-58 (56.6310; −27.5884; 2748.5 mwd) was obtained from the Iceland Basin to the East of the Reykjanes Ridge, and the deepest core BC-33 (47.2911; −20.2635; 4517.0 mwd) from the West Europe Basin, on the eastern flank of the Mid-Atlantic Ridge (see Fig. 2). All the cores were sliced every 0.5 cm for the first 10 cm and every 1 cm from centimetre 11 up to the bottom, resulting in 30 samples for BC-77, 35 samples for BC-73, 28 samples for BC-58 and 26 samples for BC-33. Sediment samples were dried at (45 ± 5) °C to constant weight, and water content was determined. The geometry selected to prepare the measuring sources was
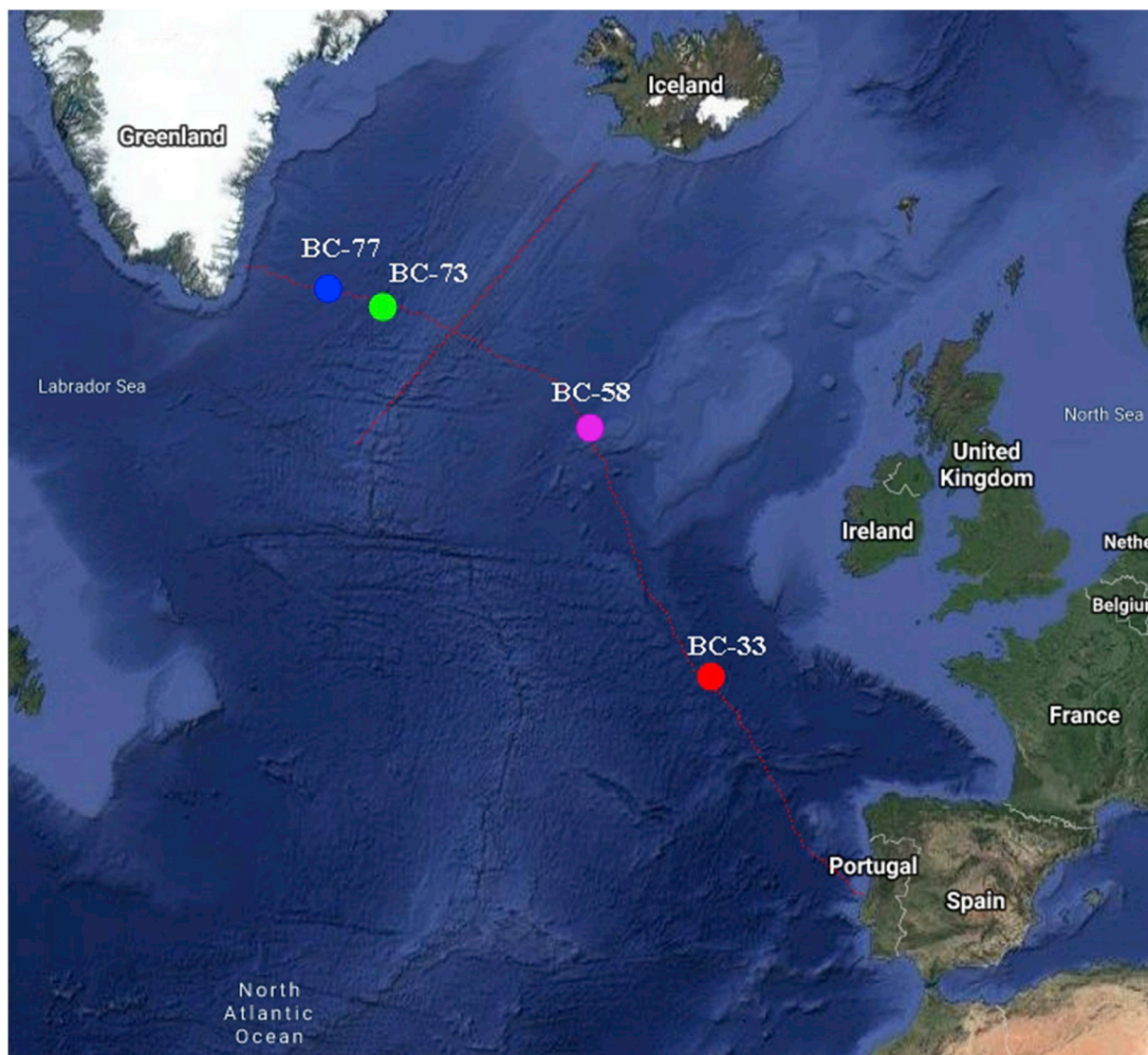

Fig. 2. Hydrographic (CTD) and sediment stations during the cruise.

Table 1

Activity concentration for ^{210}Pb, ^{214}Pb, ^{226}Ra and ^{210}Pb$_{xs}$, age and sedimentation rate (r) obtained at each depth in the sediment core BC-73.

Depth (cm)	^{210}Pb (Bq·kg^{-1})	^{214}Pb (Bq·kg^{-1})	^{226}Ra (Bq·kg^{-1})	^{210}Pb$_{xs}$ (Bq·kg^{-1})	Age (a)	r (mm·a^{-1})
1.0[a]	155.4 (51)	23.77 (73)	29.8 (54)	125.6 (74)	2009.9 (23)	0.82 (32)
1.5	125.6 (43)	29.0 (10)	31.2 (45)	96.6 (44)	2006.1 (25)	1.60 (52)
2.0	84.1 (30)	24.44 (78)	27.1 (53)	59.6 (31)	2003.0 (27)	1.46 (40)
2.5	92.1 (32)	29.12 (86)	28 (17)	62.9 (33)	1999.5 (29)	1.02 (24)
3.0	106.4 (36)	31.96 (97)	24.8 (90)	74.4 (37)	1994.6 (33)	1.37 (29)
3.5	82.1 (28)	32.40 (96)	30.1 (93)	49.7 (30)	1991.0 (36)	2.16 (44)
4.0[a]	66.8 (24)	33.27 (97)	37.6 (24)	29.2 (34)	1988.7 (39)	2.70 (54)
4.5	52.5 (19)	30.65 (90)	30.4 (63)	21.8 (21)	1986.8 (41)	6.8 (13)
5.0	43.3 (17)	35.2 (11)	36.4 (94)	8.1 (20)	1986.1 (42)	5.6 (11)
5.5	44.1 (17)	35.0 (10)	36.9 (83)	9.0 (20)	1985.2 (43)	8.0 (16)
6.0	41.7 (17)	35.1 (10)	33.4 (41)	6.5 (19)	1984.6 (43)	3.64 (71)
6.5	50.9 (19)	36.9 (11)	36.9 (49)	14.0 (22)	1983.2 (45)	1.56 (30)
7.0[a]	72.5 (27)	34.4 (10)	43.3 (26)	29.1 (37)	1980.0 (50)	1.03 (29)
7.5[a]	82.4 (29)	30.11 (95)	42.4 (69)	40.0 (75)	1975.1 (58)	2.37 (48)
8.0	53.5 (21)	37.7 (11)	36.7 (57)	15.7 (24)	1973.0 (62)	1.05 (22)
8.5	65.3 (23)	36.5 (11)	36.2 (41)	28.8 (25)	1968.3 (71)	2.61 (56)
9.0	43.1 (18)	33.46 (99)	37.3 (63)	9.7 (20)	1966.4 (75)	4.27 (92)
9.5	44.6 (18)	38.7 (12)	44.3 (71)	5.9 (22)	1965.2 (78)	6.7 (15)
10.0[a]	45.7 (18)	35.5 (10)	42.2 (53)	3.6 (5.6)	1964.4 (81)	3.64 (82)
11.0	48.2 (19)	41.8 (13)	45.4 (50)	6.4 (23)	1961.7 (89)	13.0 (30)
12.0	44.6 (18)	43.0 (13)	42.8 (47)	1.7 (22)	1960.9 (91)	3.48 (83)
13.0	47.8 (18)	4128 (12)	43.5 (35)	5.9 (21)	1958 (10)	2.64 (67)
14.0	49.3 (20)	42.8 (13)	43.8 (47)	6.5 (23)	1954 (11)	2.06 (58)
15.0[a]	53.9 (23)	39.4 (12)	46.3 (65)	7.62 (69)	1949 (14)	4.7 (14)
16.0	50.9 (20)	47.9 (14)	48.8 (46)	3.0 (24)	1947 (15)	5.4 (18)
17.0[a]	53.5 (20)	42.4 (13)	51.1 (78)	2.4 (80)	1945 (17)	15.7 (55)
18.0[a]	55.0 (20)	46.6 (13)	54.2 (66)	0.81 (68)	1945 (18)	1.94 (74)
19.0	56.0 (20)	50.0 (16)	52.2 (38)	6.0 (26)	1940 (22)	1.93 (81)
20.0	56.2 (21)	50.7 (15)	56.0 (39)	5.5 (26)	1934 (25)	0.99 (49)
21.0	56.2 (19)	48.9 (14)	54.9 (61)	7.3 (24)	1924 (35)	0.48 (34)
22.0	53.1 (19)	43.0 (13)	50.9 (35)	10.1 (23)	1904 (67)	0.15 (46)

[a] Activity concentration for ^{210}Pb$_{xs}$ calculated by subtracting the ^{226}Ra activity concentration by the ^{226}Ra direct emission.

made of two high-density polystyrene (HDPE) disks, 42 mm diameter and 6 mm height each one. The two disks are symmetrically placed in Mazinger. The vertical distance between the upper disk and the HPGe crystal placed above is 2.37 mm, the same one as between the lower disk and the HPGe crystal placed below, minimizing the distance to the detectors. The full sediment is homogenised and the disks are filled up to reaching a total mass of 15 g.

Sediment sources were measured with Mazinger, and the acquired spectra were analysed with Galea, which is a gamma spectrum analysis tool developed in our group. Its main capabilities are two: its ability to calculate a single function that represents the entire continuum of the analysed spectrum with the COSPAJ algorithm (Quintana and Fernández, 1998) and its capability to adjust peaks and multiplets using a genetic algorithm. These features are essential in the analysis of spectra from natural radionuclides because they are characterized by low-intensity peaks, which are highly overlapped, and some of them appear at low energy, where the continuum background plays an important role. Another feature is the inclusion of a library of line emissions, energy and intensity, from natural radionuclides to obtain their complete identification in the spectrum. Radionuclides activities are derived from different net peak areas, taking into account detector efficiencies, tabulated intensities and isotopic relationships.

^{210}Pb emits a gamma-ray at 46.54 keV, whose precise quantification requires a reliable baseline determination. ^{226}Ra direct emission at 186.21 keV was deconvoluted from the multiplet that shares with the ^{235}U emission at 185.72 keV. For a precise ^{226}Ra determination, emissions from the ^{226}Ra daughters were also considered, once secular equilibrium was checked. The ^{235}U activity value was also checked by using the ^{238}U activity value to verify the ^{226}Ra-^{235}U multiplet deconvolution. For the evaluation of the ^{238}U activity, peak areas at 92.38 keV and 92.83 keV, although highly overlapped, were used together with the peak area at 63.30 keV. The activity concentration calculated through ^{226}Ra direct emission served to check the secular equilibrium between

^{226}Ra and ^{214}Pb. From the evaluation of these results, ^{210}Pb$_{xs}$ activity value was calculated by subtracting the ^{226}Ra activity concentration obtained by ^{214}Pb, when fulfilled secular equilibrium, or by the ^{226}Ra direct emission, when not, to the total ^{210}Pb activity concentration to account for any textural differences among core samples (San Miguel et al., 2004). ^{210}Pb$_{xs}$ decreases according to the radioactive decay law with T$_{1/2}$ = 22.23 a and below a certain depth, its contribution is not measurable. The higher the spectrometer sensitivity, the deeper the core length in which ^{210}Pb$_{xs}$ can be determined. All sediment radionuclide concentrations were obtained in Bq/kg dry weight. Minimum detectable activities (MDA) were typically below 0.52 Bq/kg for ^{210}Pb, 0.49 Bq/kg for ^{214}Pb and 1.86 Bq/kg for ^{226}Ra.

The application of the CRS model did not require any modelling since the ages were calculated directly from the (Sánchez-Cabeza and Ruiz-Fernández, 2012; Sánchez-Cabeza et al., 2000) Eq. (1):

$$t_n = \frac{1}{\lambda_{210}} ln\left(\frac{A_s}{A_S - A_n}\right), \tag{1}$$

where n indicates depth, λ_{210} is the ^{210}Pb day constant, A_S total accumulated inventory (^{210}Pb$_{xs}$ activity accumulated) and A_n accumulated inventory up to depth n.

Once the time between samples was known, mass accumulation rates (MAR, cm·a^{-1}) can be calculated simply as the ratio of the same intervals for depth ($z_{n+1} - z_n$) and time ($t_n - t_{n+1}$) (Eq. (2)).

$$MAR_n = \frac{z_{n+1} - z_n}{t_n - t_{n+1}} \tag{2}$$

where z indicates depth and t the ages calculated.

A detector background measured during 1,272,250 s was used, with a constant flux of N$_2$ gas of 2 L/min. Mazinger background peak count rates of interest for samples were 247 (38)·10^{-6} s^{-1} at 46.54 keV for ^{210}Pb, 762 (60)·10^{-6} s^{-1} at 186 keV for ^{226}Ra and 2223 (58)·10^{-6} s^{-1} at 351.93 keV for ^{214}Pb.
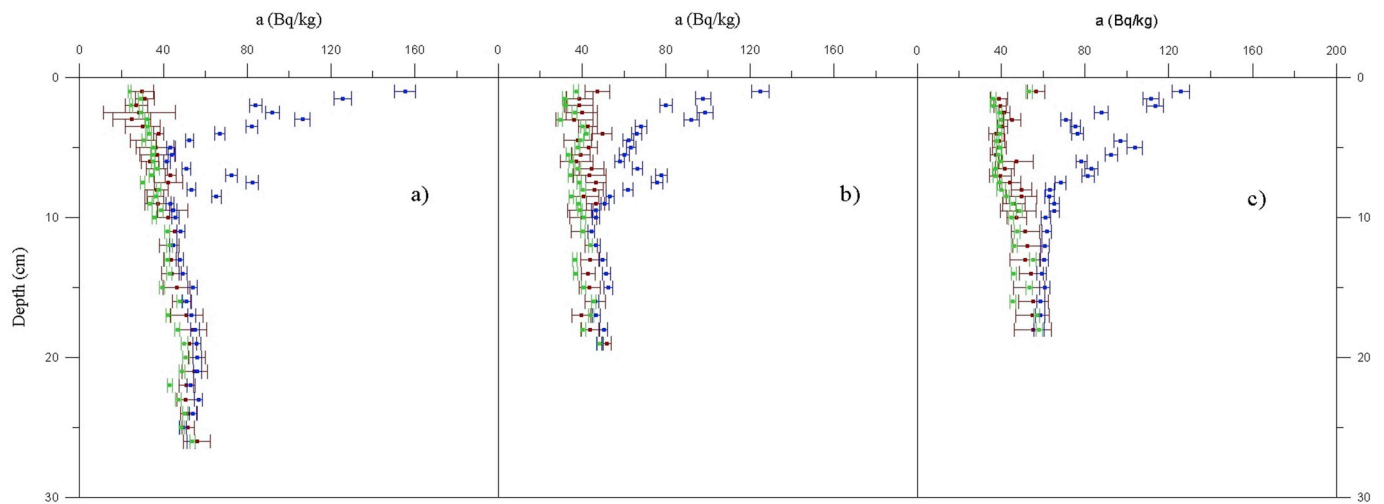
Fig. 3. (a) Specific activity concentrations (Bq/kg^{-1}) of ^{214}Pb (in green), ^{226}Ra (in red) and ^{210}Pb(in blue) versus depth for sediment cores BC-73(a); BC-58(b) and BC-33(c). (For interpretation of the references to colour in this figure legend, the reader is referred to the Web version of this article.)

Three standard radioactive solutions were used to calculate efficiencies. The first one was the multi-nuclide standard provided by AREVA, with reference number 785715/2, and containing 7.54 (15) Bq/g of ^{60}Co, 0.959 (19) Bq/g of ^{241}Am and 4.54 (91) Bq/g of ^{137}Cs. The second one contained 100.1 (18) Bq/g of ^{210}Pb and the third one, 2.387 (84) Bq/g of ^{226}Ra, both provided by CIEMAT, with references FRC-2013-00309/2 and 018–90/MTRI, respectively. The spiked sediment sources were obtained by adding the standard radioactive solution (0.5 mL of ^{210}Pb, 1 mL of multi-gamma solution and 2 mL of ^{226}Ra) on sediments selected from the ones previously measured and drying in a heater. The spiked sediment is homogenised, being the final source geometry the same one as in the original source. Full-energy peak efficiencies (FEP) obtained were 0.3090 (97) at 46.54 keV, 0.2523 (96) at 186.21 keV and 0.1638 (47) at 351.312 keV. For the anthropogenic radionuclides, the FEP obtained were 0.073 (19) for ^{137}Cs and 0.3212 (87) for ^{241}Am.

A sediment sample was used to perform the corresponding sealing tests for the study of sediments in the geometry used with high-density polystyrene. A spiked sediment source was obtained by adding 2 mL of the ^{226}Ra standard solution, drying the enriched sediment in a heater, homogenising, filling the disks, pumping down the source box and waiting 25 days to measure. An activity correlation between ^{214}Pb/^{226}Ra of 95.6 (97) % was obtained.

3. Results

The excess of ^{210}Pb with respect to ^{226}Ra and, therefore, to the ^{210}Pb$_{sup}$ fraction was observed in the vertical profiles of total ^{210}Pb, ^{214}Pb and ^{226}Ra specific activities. The specific activities for ^{210}Pb were detected in the whole dated core, with maxima at the surface and a clearly diminishing exponential profile towards deeper sediments. Specific activities, dates and sedimentation rates with their

Table 2
Activity concentration for ^{210}Pb, ^{214}Pb, ^{226}Ra and ^{210}Pb$_{xs}$, age and sedimentation rate (r) obtained at each depth in the sediment core BC-58.

Depth (cm)	^{210}Pb (Bq·kg^{-1})	^{214}Pb (Bq·kg^{-1})	^{226}Ra (Bq·kg^{-1})	^{210}Pb$_{xs}$ (Bq·kg^{-1})	Age (a)	r (mm·a^{-1})
1.0	125.0 (43)	37.1 (11)	47.2 (59)	87.9 (44)	2011.2 (20)	1.03 (42)
1.5	97.6 (36)	31.6 (10)	38.7 (64)	66.0 (38)	2008.0 (21)	1.62 (54)
2.0	80.0 (30)	32.1 (10)	38.4 (67)	47.9 (32)	2004.9 (23)	1.26 (33)
2.5	98.6 (39)	36.3 (12)	39.8 (74)	62.3 (40)	2001.0 (25)	1.12 (24)
3.0	92.1 (37)	29.6 (10)	36.2 (88)	62.5 (38)	1996.5 (28)	2.05 (40)
3.5	68.1 (28)	40.4 (13)	42.7 (68)	27.6 (31)	1994.0 (30)	3.59 (68)
4.0[a]	66.1 (24)	42.2 (11)	49.7 (47)	16.5 (53)	1992.6 (31)	2.48 (46)
4.5	62.0 (25)	39.4 (12)	37.8 (65)	22.7 (28)	1990.6 (33)	2.60 (47)
5.0[a]	63.4 (24)	37.8 (11)	43.1 (42)	20.2 (48)	1988.7 (35)	2.27 (41)
5.5[a]	60.1 (24)	33.5 (11)	39.4 (45)	20.6 (50)	1986.5 (37)	1.81 (32)
6.0	58.0 (23)	34.6 (10)	37.3 (78)	23.4 (25)	1983.7 (40)	1.62 (29)
6.5[a]	66.3 (24)	37.9 (14)	44.5 (58)	21.8 (63)	1980.7 (45)	0.95 (18)
7.0[a]	77.8 (28)	34.3 (11)	43.5 (78)	34.3 (83)	1975.4 (54)	0.92 (18)
7.5[a]	75.6 (28)	38.6 (12)	46.6 (50)	29.0 (57)	1970.0 (65)	1.34 (27)
8.0[a]	61.8 (23)	40.3 (14)	45.8 (41)	16.0 (47)	1966.2 (74)	1.05 (23)
8.5	53.3 (19)	34.7 (10)	40.7 (71)	18.6 (22)	1961.5 (85)	3.90 (87)
9.0[a]	50.8 (19)	38.2 (11)	46.4 (45)	4.4 (49)	1960.2 (90)	2.22 (51)
9.5	46.4 (19)	38.9 (12)	39.1 (59)	7.6 (22)	1957.9 (96)	2.56 (61)
10.0	46.6 (18)	40.5 (12)	40.5 (65)	6.1 (22)	1956 (10)	3.40 (85)
11.0	44.3 (17)	40.3 (12)	40.2 (56)	4.0 (20)	1953 (11)	4.6 (12)
12.0	46.7 (18)	43.89 (89)	44.2 (30)	2.8 (20)	1951 (12)	1.99 (57)
13.0[a]	49.8 (19)	36.4 (11)	43.9 (45)	5.9 (59)	1946 (15)	1.11 (37)
14.0[a]	51.4 (19)	36.7 (10)	42.9 (34)	8.6 (39)	1937 (20)	0.46 (22)
15.0	52.4 (21)	40.6 (11)	43.5 (50)	11.8 (24)	1915 (41)	5.9 (34)
16.0	46.2 (17)	45.5 (11)	46.2 (49)	0.7 (20)	1913 (43)	1.44 (93)

[a] Activity concentration for ^{210}Pb$_{xs}$ calculated by subtracting the ^{226}Ra activity concentration by the ^{226}Ra direct emission.
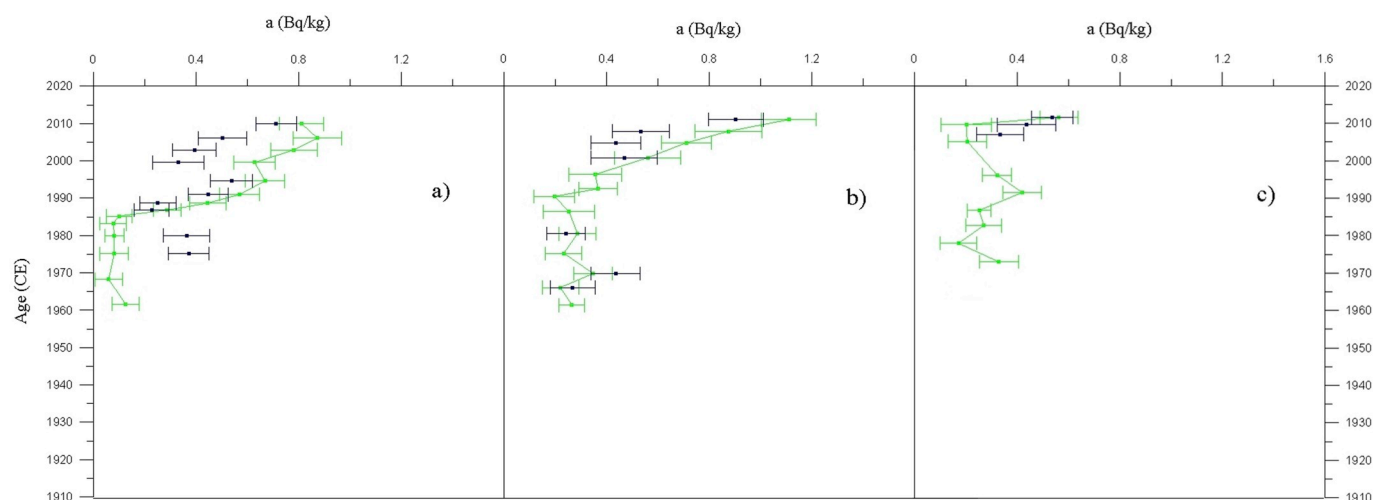
Fig. 4. (a) Specific activity concentrations (Bq/kg^{-1}) of ^{137}Cs (in green) and ^{241}Am (in blue) versus age (a) for the sediment cores BC-73(a); BC-58(b) and BC-33(c). (For interpretation of the references to colour in this figure legend, the reader is referred to the Web version of this article.)

Table 3
Activity concentration for ^{210}Pb, ^{214}Pb, ^{226}Ra and ^{210}Pb$_{xs}$, age and sedimentation rate (*r*) obtained at each depth in the sediment core BC-33.

Depth (cm)	^{210}Pb (Bq·kg^{-1})	^{214}Pb (Bq·kg^{-1})	^{226}Ra (Bq·kg^{-1})	^{210}Pb$_{xs}$ (Bq·kg^{-1})	Age (a)	r (mm·a^{-1})
1.0	125.6 (42)	53.3 (15)	56.6 (41)	72.2 (44)	2011.6 (17)	1.14 (45)
1.5	111.5 (40)	36.3 (11)	38.9 (42)	75.2 (41)	2009.6 (18)	1.95 (69)
2.0[a]	113.5 (39)	36.0 (11)	39.5 (29)	74.0 (49)	2007.1 (19)	2.64 (74)
2.5	87.8 (32)	39.2 (12)	41.4 (26)	48.6 (34)	2005.2 (20)	4.0 (10)
3.0[a]	71.0 (25)	40.1 (12)	45.1 (42)	26.0 (49)	2003.9 (21)	2.61 (60)
3.5	75.4 (26)	39.1 (11)	40.7 (25)	36.3 (28)	2002.0 (22)	2.39 (50)
4.0	76.4 (29)	39.2 (12)	37.7 (38)	37.2 (31)	1999.9 (23)	1.34 (25)
4.5	96.8 (32)	38.0 (11)	38.8 (30)	58.8 (34)	1996.2 (25)	1.06 (18)
5.0	103.7 (35)	39.2 (12)	39.0 (32)	64.6 (37)	1991.5 (28)	1.05 (17)
5.5	92.6 (31)	38.7 (11)	37.6 (28)	53.8 (33)	1986.7 (32)	1.25 (19)
6.0	78.3 (27)	39.6 (12)	47.1 (81)	38.7 (30)	1982.7 (36)	1.04 (16)
6.5[a]	83.1 (30)	37.1 (11)	41.7 (54)	41.4 (54)	1977.9 (42)	1.01 (16)
7.0	81.4 (30)	37.2 (12)	39.6 (53)	44.2 (32)	1973.0 (49)	1.10 (18)
7.5[a]	68.3 (26)	39.3 (12)	44.3 (49)	24.0 (55)	1968.4 (57)	2.03 (35)
8.0[a]	63.3 (22)	39.9 (20)	49.7 (49)	13.6 (54)	1966.0 (62)	1.90 (34)
8.5[a]	63.0 (24)	42.4 (13)	49.6 (73)	13.3 (76)	1963.3 (69)	1.29 (25)
9.0	65.3 (24)	45.6 (13)	46.0 (55)	19.7 (27)	1959.5 (78)	1.26 (25)
9.5	65.4 (25)	48.6 (14)	48.2 (84)	16.8 (28)	1955.5 (88)	0.96 (21)
10.0	61.3 (22)	44.7 (12)	47.4 (47)	16.5 (25)	1950 (10)	0.98 (24)
11.0	61.7 (22)	47.6 (14)	51.6 (67)	14.1 (26)	1940 (14)	0.62 (20)
12.0	60.8 (22)	46.2 (13)	52.4 (70)	14.6 (26)	1924 (24)	1.14 (47)
13.0	60.4 (22)	55.1 (16)	51.5 (72)	5.3 (27)	1915 (32)	0.97 (51)
14.0[a]	59.3 (23)	46.1 (13)	54.4 (58)	5.0 (62)	1905 (47)	0.32 (31)
15.0	60.8 (23)	53.4 (16)	53.4 (74)	7.4 (28)	1874 (125)	0.28 (69)

[a] Activity concentration for ^{210}Pb$_{xs}$ calculated by subtracting the ^{226}Ra activity concentration by the ^{226}Ra direct emission.

correspondent uncertainties obtained by applying the CRS model are shown in Fontela et al. (2019) for BC-77 and in Tables 1–3 for the rest of cores.

The maximum activity concentration of ^{210}Pb is observed in the first centimeter of the sediment cores, with values of 155.4 (51) Bq·kg^{-1}, 125.0 (43) Bq·kg^{-1} and 125.6 (42) Bq·kg^{-1} while minima one is found at 6 cm depth with a value of 41.7 (17) Bq·kg^{-1}, at 11 cm depth, with a value of 44.3 (17) Bq·kg^{-1} and at 18 cm depth, with a value of 58.1 (23) Bq·kg^{-1}, for BC-73, BC-58 and BC-33 respectively, as shown in Fig. 3.

The complete total ^{210}Pb$_{xs}$ inventory was determined as 4.03 (18) kBq·m^{-2}, what gives a corresponding flux of 35.8 (27) Bq·m^{-2}·a^{-1} for BC-73, of 2.48 (10) kBq·m^{-2}, what gives a corresponding flux of 24.2 (23) Bq·m^{-2}·a^{-1} for BC-58 and of 4.20 (15) kBq·m^{-2}, what gives a corresponding flux of 29.5 (12) Bq·m^{-2}·a^{-1} for BC-33. A maximum dated period between 100 and 150 years was established by applying the CRS model. In this case, ^{210}Pb in excess reached up to 22 cm with estimated date of 1904 (67) CE, up to centimetre 16 cm with estimated

date of 1913 (43) CE and up to centimetre 15 cm with estimated date of 1874 (125) CE, for BC-73, BC-58 and BC-33 respectively.

The highest specific activity in the ^{137}Cs profile of the BC-73 core, 0.873 (94) Bq·kg^{-1}, was obtained in the first centimetre, which was ^{210}Pb$_{xs}$ dated 2009.9 (23) CE as shown in Table 1. The same one as for BC-58 and BC-33, being their specific activities 1.11 (11) Bq·kg^{-1} and 0.563 (73) Bq·kg^{-1} and ages of 2011.2 (20) CE as shown in Table 2 and 2011.6 (17) CE as shown in Table 3, respectively. The maximum specific activity detected for ^{241}Am was 0.713 (79) Bq·kg^{-1} at 1.5 cm of depth for BC-73, 0.90 (11) Bq·kg^{-1} at 1 cm of depth for BC-58 and 0.537 (80) Bq·kg^{-1} at 1 cm of depth. The first detection of ^{241}Am was: for BC-73 the shallowest detection of ^{241}Am was near 1975.1 (58) CE, and ^{137}Cs was detected until the depth corresponding with the year 1961.7 (89) CE, for BC-58 the first detection of ^{241}Am was near 1966.2 (74) CE and ^{137}Cs was detected until the depth corresponding with the year 1961.5 (85) CE and for BC-33 the first detection of ^{241}Am was near 2007.1 (19) CE and ^{137}Cs was detected until the depth corresponding with the year 1973.0
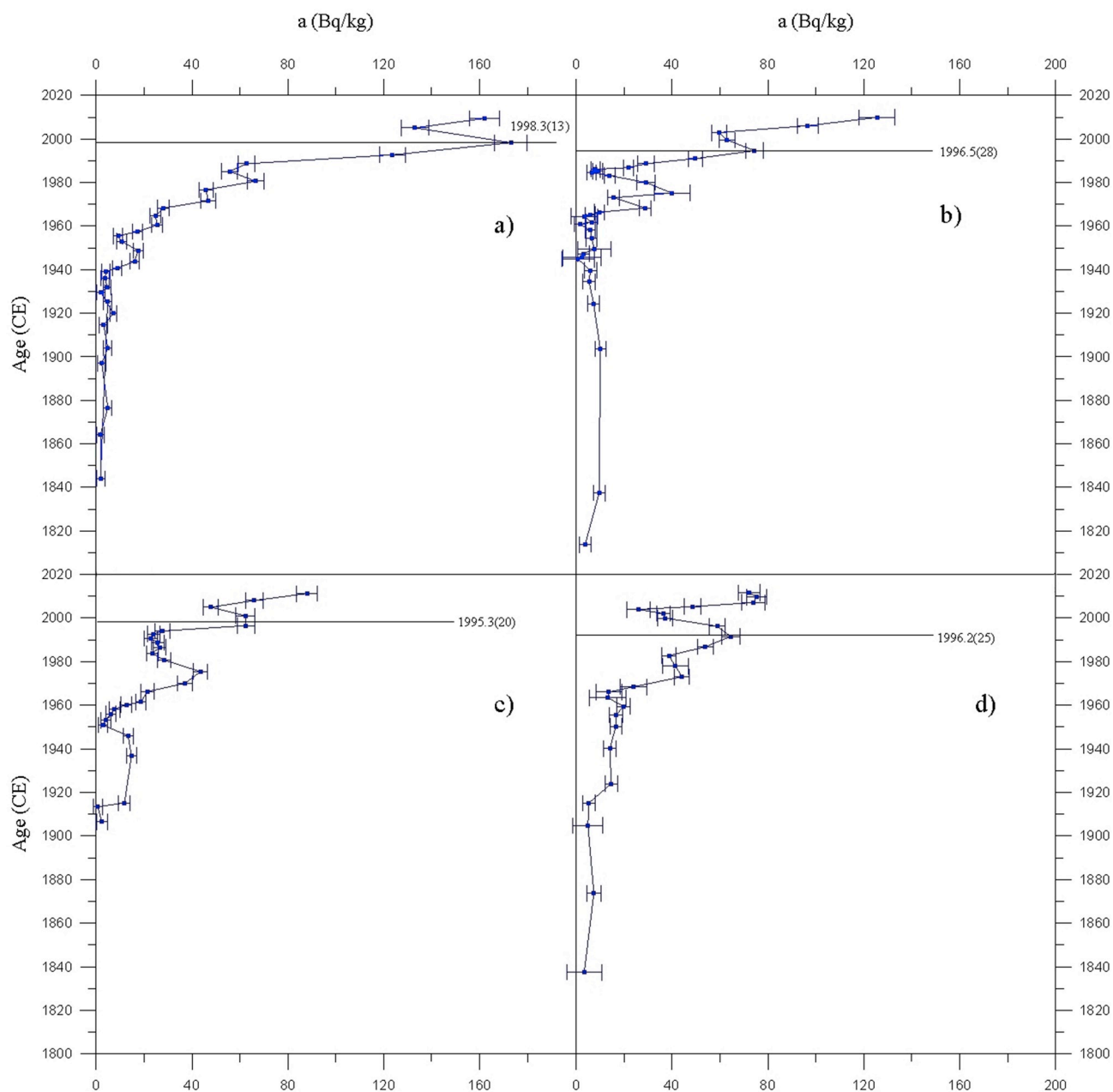
Fig. 5. Specific activity profile of $^{210}Pb_{xs}$ versus age (a) for the sediment cores BC-77(a); BC-73(b); BC-58(c) and BC-33(d).

(49) CE, as seen in Fig. 4.

4. Discussion

The $^{210}Pb_{xs}$ specific activity profile did not show a steady exponential behaviour in the three cores, making the CRS model to be the only choice to date the sediments. As in Fontela et al. (2019), it was also shown that Mazinger, with its high efficiency and very low background, was accurate and sensitive enough to date high-resolution deep-sea sediments because the trend towards zero excess of the $^{210}Pb_{xs}$ profile could be measured in BC-73, BC-58 and BC-33.

The obtained $^{210}Pb_{xs}$ fluxes to the bottom were similar in the three cores, as expected, given that they came from the same region (Masqué et al., 2002). Our flux estimates, from 25.15 (38) to 33.05 (38) $Bq·m^{-2}·a^{-1}$, agreed with the atmospheric fallout values for far land-masses sites from 30 to 40 $Bq·m^{-2}·a^{-1}$ (Appleby, 1998). Activity concentrations found for ^{137}Cs and ^{241}Am were close to the detection

limits and weren't detectable in the environment before 1952. (Povinec et al., 2003). However, ^{137}Cs has post-depositional diagenetic mobility (Sholkovitz and Mann, 1984), limiting the resolution of specific dates (Fontela et al., 2019). The maxima in the ^{137}Cs profile closer to the top for the three sediment cores agreed with the Fukushima nuclear accident's date, March 11th, 2011 (Buesseler et al., 2011). This event was registered in all the profiles due very likely to the short time elapsed between sampling and accident, which was not enough to smooth the peak in the ^{137}Cs profiles because of migration. From this level to the bottom, the post-depositional diagenetic mobility is observed in the three sediment cores.

In all the $^{210}Pb_{xs}$ profiles, the main maximum was observed in the first centimetre along with other sub-maxima in deeper intervals. Cores were sampled to both sides of the Reykjanes Ridge, which goes across Iceland, where the tectonic activity is very high in the area, producing both earthquakes and volcanic eruptions. These volcanic eruptions in Iceland produce subaerial particles due to the volcanic ash which are

deposited in the nearby basins. For example, the volcanic lake Grímsvötnin caused in 1996 one violent event due to the contact between volcanic eruptions and glaciers, which could influence the $^{210}Pb_{xs}$ profiles of the sediment cores.

Fig. 5 shows $^{210}Pb_{xs}$ profile versus age (CE) in sediment core BC-77 for comparison with the other three dated in this work. In BC-77, the maximum activity in the peaked shape of the profile was found to correspond to 1998.3 (13) CE; in the sediment core BC-73, the same maximum was dated 1996.5 (28) CE. Eastwards of the ridge, the sediment cores BC-58 and BC-33 registered the same event in 1995.3 (20) CE and 1996.2 (25) CE. This fact implied that the method used to carry out the dating in the four sediments cores was suitable and provided reliable ages.

5. Conclusions

In this study ^{210}Pb-dating in three sediments cores of paleoclimate interest from remote basins of deep waters of the North Atlantic were performed by using Mazinger, the gamma spectrometer of high efficiency and very low background, designed and optimized in our group. An excellent consistency was found between dating and recent history of the area of study, but also regarding $^{210}Pb_{xs}$ inventories and fluxes. The results show that Mazinger can be used for ^{210}Pb-dating marine sediments from very deep areas where the sedimentation rates are very low.

Funding

Declaration of competing interest

The authors declare that they have no known competing financial interests or personal relationships that could have appeared to influence the work reported in this paper.

References

Alvarez-Iglesias, P., Quintana, B., Rubio, B., Pérez-Arlucea, M., 2007. Sedimentation rates and trace metal input history in intertidal sediments from San Simon Bay (Ria de Vigo, NW Spain) derived from ^{210}Pb and ^{137}Cs chronology. J. Environ. Radioact. 98, 229–250. https://doi.org/10.1016/j.jenvrad.2007.05.001.
Alvarez-Vázquez, M.A., Caetano, M., Alvarez-Iglesias, P., del Canto Pedrosa-García, M., Calvo, S., De Una-Alvarez, E., Quintana, B., Vale, C., Prego, R., 2016. Natural and Anthropocene fluxes of trace elements in estuarine sediments of Galician Rias. Estuar. Coast Shelf Sci. https://doi.org/10.1016/j.ecss.2016.08.022.
Appleby, P.G., 1998. Dating recent sediments by ^{210}Pb: problems and solutions. STUK-A 145, 7–24. https://inis.iaea.org/collection/NCLCollectionStore/_Public/29/040/29040426.pdf.
Appleby, P.G., Oldfield, F., 1983. The assessment of ^{210}Pb data from sites with varying sediment accumulation rates. Hydrobiologia 103, 29–35. https://doi.org/10.1007/BF00028424.

Bé, M., Chisté, V., Dulieu, C., Chechev, V., Kuzmenko, N., Galan, M., 2011. Table of Radionuclides. LNHB. CEA 0002-9343(57)90323-6. https://www.bipm.org/utils/common/pdf/monographieRI/Monographie_BIPM-5_Comments_Vol1-5.pdf.
Britton, R., Davies, A.V., Burnett, J.L., Jackson, M.J., 2015. A high-efficiency HPGe coincidence system for environmental analysis. J. Environ. Radioact. 146, 1–5. https://doi.org/10.1016/j.jenvrad.2015.03.033.
Buesseler, K., Aoyama, M., Fukasawa, M., 2011. Impacts of the Fukushima nuclear power plants on marine radioactivity. Environ. Sci. Technol. 45, 9931–9935. https://doi.org/10.1021/es202816c.
Chen, H.Y., Huh, C.A., 1999. ^{232}Th-^{228}Ra-^{228}Th disequilibrium in East China Sea sediments. J. Environ. Radioact. 42, 93–100. https://doi.org/10.1016/S0265-931X(98)00030-7.
Fontela, M., Francés, G., Quintana, B., Alvarez-Fernández, M.J., Nombela, M.A., Alejo, I., Pedrosa, M.C., Pérez, F., 2019. Dating the Anthropocene in deep-sea sediments: how much carbon is buried in the Irminger Basin? Glob. Planet. Chang. 175, 92–102.
Hassan, A.M., Abdel-Wahab, M., Nada, A., Walley El-Dine, N., Khazbak, A., 1997. Determination of uranium and thorium in Egyptian monazite by gamma-ray spectrometry. Appl. Radiat. Isot. 48, 149–152. https://doi.org/10.1016/S0969-8043(96)00063-2.
Irabien, M.J., Garcia-Artola, A., Cearreta, A., Leorri, E., 2015. Chemostratigraphic and lithostratigraphic signatures of the Anthropocene in estuarine areas from the eastern Cantabrian coast (N. Spain). Quat. Int. 364, 196–205. https://doi.org/10.1016/j.quaint.2014.08.056.
Krishnaswamy, S., Lal, D., Martin, J.M., Meybeck, M., 1971. Geochronology of lake sediments. Earth Planet. Sci. Lett. 11, 407–414. https://doi.org/10.1016/0012-821X(71)90202-0.
Leorri, E., Mitra, S., Irabien, M.J., Zimmerman, A.R., Blake, W.H., Cearreta, A., 2014. A 700 year record of combustion-derived pollution in northern Spain: tools to identify the Holocene/Anthropocene transition in coastal environments. Sci. Total Environ. 470–471, 240–247. https://doi.org/10.1016/j.scitotenv.2013.09.064.
Mabit, L., Benmansour, M., Abril, J.M., Walling, D.E., Meusburger, K., Iurian, A.R., Bernard, C., Tarjan, S., Owens, P.N., Blake, W.H., Alewell, C., 2014. Fallout ^{210}Pb as a soil and sediment tracer in catchment sediment budget investigations: a review. Earth Sci. Rev. 138, 335–351. https://doi.org/10.1016/j.earscirev.2014.06.007.
Manolopoulou, M., Stoulos, St, Mironaki, D., Papastefanou, C., 2003. A new technique for the accurate measurement of ^{226}Ra by gamma spectrometry in voluminous samples. Nucl. Instrum. Methods A 508, 362–366. https://doi.org/10.1016/S0168-9002(03)01701-7.
Masqué, P., Isla, E., Sánchez-Cabeza, J.A., Palanques, A., Bruach, J.M., Puig, P., Guillen, J., 2002. Sediment accumulation rates and carbon fluxes to bottom sediments at the western Bransfield Strait (Antarctica). Deep Sea Res. Part II Top. Stud. Oceanogr. 49, 921–933. https://doi.org/10.1016/S0967-0645(01)00131-X.
Povinec, P.P., Bailly du Bois, P., Kershaw, P.J., Nies, H., Scotto, P., 2003. Temporal and spatial trends in the distribution of 137Cs in surface waters of Northern European Seas - a record of 40 years of investigations. Deep Sea Res. Part II Top. Stud. Oceanogr. 50, 2785–2801. https://doi.org/10.1016/S0967-0645(03)00148-6.
Quintana, B., Fernández, F., 1998. Continuous component determination in γ-ray spectra. Nucl. Instrum. Methods Phys. Res. Sect. A Accel. Spectrom. Detect. Assoc. Equip. 411, 475–493. https://doi.org/10.1016/S0168-9002(98)00334-9.
Quintana, B., Pedrosa, C., Bombin, R., Martin, S., Lozano, J.C., 2017. Mazinger, a γ-ray spectrometry system of high efficiency and very low background for paleoclimate applications. Appl. Radiat. Isot. 126, 116–120. https://doi.org/10.1016/j.apradiso.2017.02.017.
Quintana, B., Pedrosa, M.C., Vázquez-Canelas, L., Santamaría, R., Sanjuan, M.A., Puertas, F., 2018. A method for the complete analysis of NORM building materials by γ-ray spectrometry using HPGe detectors. Appl. Radiat. Isot. 134, 470–476. https://doi.org/10.1016/j.apradiso.2017.07.045.
San Miguel, E.G., Bolívar, J.P., García-Tenorio, R., 2004. Vertical distribution of Th-isotope ratios, ^{210}Pb, ^{226}Ra and ^{137}Cs in sediment cores from an estuary affected by anthropogenic releases. Sci. Total Environ. 318 (Issues 1–3), 143–157. https://doi.org/10.1016/S0048-9697(03)00367-X.
Sánchez-Cabeza, J.A., Ani-Ragolta, I., Masque, P., 2000. Some considerations of the ^{210}Pb constant rate of supply (CRS) dating model. Limnol. Oceanogr. 45, 990–995. https://doi.org/10.4319/lo.2000.45.4.0990.
Sánchez-Cabeza, J.A., Ruiz-Fernández, A.C., 2012. ^{210}Pb sediment radiochronology: an integrated formulation and classification of dating models. Geochem. Cosmochim. Acta 82, 183–200. https://doi.org/10.1016/j.gca.2010.12.024.
Sholkovitz, E.R., Mann, D.R., 1984. The pore water chemistry of Pu-239,-240 and Cs-137 in sediments of Buzzards Bay, Massachusetts. Geochem. Cosmochim. Acta 48, 1107–1114. https://doi.org/10.1016/0016-7037(84)90201-1.